Far-infrared investigation of band-structure parameters and exchange interaction in $Pb_{1-x}Eu_xTe$ films

G. Karczewski* and J. K. Furdyna
Department of Physics, University of Notre Dame, Notre Dame, Indiana 46556

D. L. Partin, C. N. Thrush, and J. P. Heremans
Physics Department, General Motors Research Laboratories, Warren, Michigan 48090-9055
(Received 4 May 1992)

Far-infrared (FIR) magnetotransmission has been investigated in molecular-beam-epitaxy-grown $Pb_{1-x}Eu_xTe$ films with Eu concentration $x=0.02$. The experiments were carried out at fixed FIR photon energies between 2.5 and 21.4 meV, in the temperature range $1.8 \le T \le 60$ K, and in magnetic fields up to 6 T. From the magnetic-field dependence of the cyclotron-resonance energies the momentum matrix elements have been determined within the framework of the Mitchell-Wallis $\mathbf{k}\cdot\mathbf{p}$ model: $2P_t^2/m_0=8.23\pm0.02$ eV and $2P_l^2/m_0=0.55\pm0.02$ eV. The results signal a strong increase of band anisotropy due to the presence of Eu, from $P_t^2/P_l^2=10.3$ for pure PbTe to $P_t^2/P_l^2=14.9$ for $Pb_{0.98}Eu_{0.02}Te$. The low-field approximation of the model yields the following components of the effective-mass tensors: $m_t^v/m_0=0.023$, $m_l^v/m_0=0.287$, $m_t^c/m_0=0.020$, and $m_l^c/m_0=0.218$. A resonant transition from shallow acceptor states to valence band has also been observed. The analysis of these transitions in finite magnetic fields provided the value of the valence-band g factor, $g_t^v=15.9$. This in turn served to place an upper limit on the valence-band exchange integral α, $\alpha=-7.5\pm5.5$ meV. The small value of α indicates that the hole-Eu exchange interaction in the $Pb_{1-x}Eu_xTe$ system is at least one order of magnitude weaker than the hole-Mn interaction in $Pb_{1-x}Mn_xTe$, and two orders of magnitude below exchange parameters in $II_{1-x}Mn_xVI$ systems.

I. INTRODUCTION

Lead salt alloys have been of great importance as materials for infrared diode lasers commonly used in molecular spectroscopy, in heterodyne detection, and in trace gas analysis. Because of the rapid increase of their energy gaps with Eu^{2+} content $Pb_{1-x}Eu_xTe$ and $Pb_{1-x}Eu_xSe$ alloys constitute attractive candidates for laser materials in the mid-infrared energy region.[1] Both of these alloys, and their quaternary relative $Pb_{1-x}Eu_xTe_{1-y}Se_y$, are also used for energy barriers in multi-quantum-well $Pb_{1-x}Eu_xTe_{1-y}Se_y$/PbTe and $Pb_{1-x}Eu_xTe_{1-y}Se_y$/PbSe heterostructure devices.[2-4]

In addition to its practical importance, $Pb_{1-x}Eu_xTe$ is an interesting material from the point of view of basic physical properties. Because of the substitution of the group-IV ions by paramagnetic Eu^{2+} ions, $Pb_{1-x}Eu_xTe$ belongs to the family of diluted magnetic semiconductors (DMS's). This group of materials has attracted attention due to the exchange interaction between localized magnetic moments and quasifree carriers,[5,6] and it would be important to establish the extent to which such processes occur in $Pb_{1-x}Eu_xTe$.

Lead chalcogenides and rare-earth chalcogenides both crystallize in fcc structures, and therefore are expected to form solid solutions in a wide range of compositions. In fact, first studies of $Pb_{1-x}Eu_xTe$ alloys confirmed that EuTe is soluble in PbTe in the entire composition range $0 \le x \le 1$.[7] Films of particularly good quality have been grown for $x<0.30$ by hot-wall epitaxy and by molecular-beam epitaxy (MBE).[8,9] Recently, the coevaporation technique has also been applied for growing films with higher values of x ($0<x<0.55$).[10]

Band-structure investigations of $Pb_{1-x}Eu_xTe$ have so far not been systematically carried out, with the exception of a few reports concerning energy-gap measurements.[8-11] Early work on thin films of $Pb_{1-x}Eu_xTe$, which deduce the value of x on the basis of Vegard's law, indicated an increase of the optical gap with increasing x.[11] This conclusion was later confirmed by measurements of $Pb_{1-x}Eu_xTe$ diode laser emission.[8,9] In contrast, in the case of the $Pb_{1-x}Eu_xSe$ family of alloys, systematic studies of the band-structure parameters were recently performed, and a consistent set of band parameters has been found in the context of the $\mathbf{k}\cdot\mathbf{p}$ model.[12,13]

The aim of this paper is to determine the band-structure parameters of $Pb_{1-x}Eu_xTe$ films and to look for evidence of spin-spin exchange interaction between free carriers and localized Eu ions. We applied one of the classical and most direct experimental methods used for this type of investigation: far-infrared magnetotransmission. This method is capable of providing very precise information about the effective masses and, to a more limited extent, also on the g factors of the material under investigation. For a proper interpretation of the experimental data obtained in the presence of an external magnetic field, additional information about the magnetization of the material is required, since in DMS's the exchange interaction (which is proportional to the magnetization) is, in principle, expected to play a role. The magnetization and magnetic susceptibility of $Pb_{1-x}Eu_xTe$

have been recently measured.[14–16] It was established that the antiferromagnetic interaction between the Eu^{+2} ions in IV-VI materials is much weaker than the Mn^{2+}-Mn^{2+} interaction in both II-VI and IV-VI semiconductors. One would therefore expect a rather small influence of the exchange interaction on the band structure of $Pb_{1-x}Eu_xTe$, and one of the objectives of the paper is to determine an upper limit of this process.

The structure of this paper is as follows. Experimental details are presented in Sec. II. In Sec. III we briefly review the band structure of IV-VI compounds, including the role of exchange interaction in these materials. The results of the magnetotransmission experiments are given in Sec. IV. The analysis and discussion of the results are presented in Sec. V, and the main conclusions of the present study are summarized in Sec. VI.

II. EXPERIMENT

The $Pb_{1-x}Eu_xTe$ films used in the present study were prepared by molecular-beam epitaxy on $BaF_2(111)$ surfaces at General Motors Research Laboratories. The thickness of the films was around 2 μm. Three $Pb_{1-x}Eu_xTe$ films were available to us, with $x=0.02$, 0.034, and 0.044. The Eu concentration in the films was determined by electron microprobe analysis, with uncertainty in the x value estimated to be less than $\Delta x<0.005$.

The $Pb_{1-x}Eu_xTe$ films were further characterized by standard electrical transport measurements. All films were p type, with room-temperature hole concentrations of 1.7×10^{17}, 7.5×10^{16}, and 3.7×10^{16} cm^{-3} for $x=0.020$, 0.034, and 0.044, respectively. With decreasing temperature, the hole concentrations decreased exponentially. For the two samples with higher Eu content, the temperature freeze-out of holes was observed at about $T=150$ K. The hole concentration in the $x=0.020$ films saturated at low temperatures, reaching a value of 7.5×10^{17} cm^{-3}. The hole activation energy derived from the transport measurements appears to be extremely sensitive to the Eu content: $E_A=4.2$, 51.7, and 80.7 meV for the alloy compositions of $x=0.020$, 0.034, and 0.044, respectively. The carrier mobility increases with decreasing temperature, from 1000 cm^2/Vs at $T=300$ K to 30 000 cm^2/Vs at liquid-helium temperatures for $x=0.020$.

The far-infrared (FIR) magnetotransmission investigation was carried out on epilayers with Eu concentration $x=0.020$. We have also attempted magnetotransmission studies on other specimens, with higher Eu concentrations ($x=0.034$ and 0.044). Unfortunately, these specimens did not exhibit any FIR resonances, probably because of carrier freeze-out on deep acceptor states. Attempts to excite carriers into the bands by cw illumination with visible light also did not succeed (i.e., we did not observe any cyclotron resonance absorption). This may be indicative of very short carrier lifetimes in the samples with higher Eu concentration.

In the present investigation we studied FIR magnetotransmission at several discrete energies between 21.4 and 2.5 meV. Coherent radiation in this energy range was obtained from a CO_2-pumped FIR laser (Apollo Lasers, model 120). The measurements were carried out in both the Faraday geometry (where the propagation vector **q** of the FIR radiation and the magnetic-field direction **B** are parallel and are both normal to the sample plane) and in the Voigt geometry (where **q** is normal to the sample plane and **B** lies in the sample plane). The incident radiation was circularly polarized in the former and linearly polarized in the latter configuration. We follow the convention that the circular polarization which elicits cyclotron resonance of electrons is designated as "cyclotron resonance active" (CRA) and the opposite circular polarization is designated as "cyclotron resonance inactive" (CRI). In the Voigt geometry, the electric field **E** of the linearly polarized light was either parallel or perpendicular to the stationary magnetic-field **B**. The samples were immersed in superfluid helium or situated in an exchange-gas chamber of the optical Dewar at the center of a split-coil superconducting solenoid. The measurements were performed in a magnetic field up to $B=6$ T, mostly at $T=1.8$ K. However, the temperature dependence of FIR spectra for several laser energies was also measured (up to $T=60$ K). The samples were oriented with respect to the applied magnetic field as follows: in the Faraday geometry $\mathbf{B}\parallel[111]$, in the Voigt geometry $\mathbf{B}\parallel[1\bar{1}0]$ and $\mathbf{B}\parallel[11\bar{2}]$. The samples were oriented with respect to these orientations with an accuracy of $\pm2°$.

III. THE BAND MODEL

We assume that in $Pb_{1-x}Eu_xTe$, as in other DMS's, the substitutional addition of a small concentration of magnetic Eu^{2+} ions into the nonmagnetic PbTe lattice does not lead to qualitative changes in the band structure of the host material. The band structure of lead chalcogenides, and in particular of PbTe, has been the subject of numerous experimental and theoretical investigations.[17–20] PbTe is a direct-gap semiconductor with the narrow-band gap of $E_g=189$ meV at low temperatures. The band edges are located at the L point of the Brillouin zone. At the L point there are also two pairs of bands located about 2 eV above and below the gap region. Other bands are removed by about 8 eV from these six bands, and can thus be neglected in calculations relevant to the FIR investigations. Due to the narrowness of the energy gap the electronic dispersion relation is highly nonparabolic for both the valence and the conduction bands. For low carrier concentrations, the surfaces of constant energy consist of four highly elongated ellipsoids of revolution along the four [111] axes.

In the presence of a magnetic field the energies of the Landau states are conveniently described by the Mitchell-Wallis $\mathbf{k}\cdot\mathbf{p}$ model. This model treats the interaction of the uppermost valence-band and the lowest conduction-band level exactly, whereas the interaction with the four more distant conduction and valence bands is treated in the k^2 approximation. The 4×4 matrix Hamiltonian for the calculation of the Landau states resulting from this procedure is given in Ref. 20. The eigenvalue problem can be solved exactly only for $\mathbf{B}\parallel[111]$.

The energies of the Landau levels as a function of mag-

netic field are described by three near-band parameters (the energy gap E_g and the longitudinal and perpendicular momentum matrix elements P_l and P_t) and by eight far-band parameters ($m_{l,t}^{\pm}$ and $g_{l,t}^{\pm}$). The far-band parameters represent the contributions to the effective masses and to the g factors of the conduction and the valence bands (labeled by the superscript $-$ and $+$, respectively) resulting from the interaction of the conduction- and valence-band states with the more distant bands. For an arbitrary nonzero angle Φ between the direction of the magnetic field **B** and the [111] axis, the matrix Hamiltonian cannot be solved exactly. Approximate solutions of the eigenvalue problem are reviewed in Ref. 20. In this paper, we will apply the approximation developed by Adler, Hewes, and Senturia.[19]

For low carrier concentrations and in low magnetic fields, where the cyclotron splitting is much lower than the energy gap of the material ($\hbar\omega_c \ll E_0$), the nonparabolicity of the conduction and the valence bands is negligible and the bands can be described by parabolic dispersion relations. In this low-field approximation the band parameters are independent of magnetic field and are related to the parameters of the Mitchell-Wallis model by the following equations:

$$\begin{aligned} &m_0/m_{t,l}^{v}=2P_{t,l}^2/E_g m_0+m_0/m_{t,l}^{+} , \\ &m_0/m_{t,l}^{c}=2P_{t,l}^2/E_g m_0+m_0/m_{t,l}^{-} , \\ &g_t^{v,c}=4P_tP_l/E_g m_0+g_t^{\pm} , \\ &g_l^{v,c}=4P_t^2/E_g m_0+g_l^{\pm} . \end{aligned} \tag{1}$$

This approximation is very useful for a preliminary analysis of the magnetotransmission data.

The effect of the exchange coupling between the free electrons and the localized spins on the band structure of the DMS's is usually treated assuming the mean-field approximation.[5] In case of a PbTe-based DMS, for an arbitrary angle Φ, the exchange interaction is described by an exchange matrix of the form given below, which has to be added to the 4×4 $\mathbf{k}\cdot\mathbf{p}$ Hamiltonian,[21–23]

$$\tfrac{1}{2}xS_0B_{7/2}[7\mu_{\mathrm{B}}B/k_{\mathrm{B}}(T+T_0)]\begin{bmatrix} a & c & 0 & 0 \\ c & -a & 0 & 0 \\ 0 & 0 & b & d \\ 0 & 0 & d & -b \end{bmatrix} , \tag{2}$$

where x is the crystal composition and $B_{7/2}(\ )$ is the so-called modified Brillouin function with the argument given in parentheses in Eq. (2). The parameters S_0 and T_0 are taken from fits to the experimental magnetization data on $Pb_{1-x}Eu_xTe$.[15,16] The elements appearing in the matrix are given by

$$\begin{aligned} a &= A\cos\Phi\cos\gamma + a_1\sin\Phi\sin\gamma , \\ c &= -A\cos\Phi\sin\gamma + a_1\sin\Phi\cos\gamma , \\ b &= B\cos\Phi\cos\gamma - b_1\sin\Phi\sin\gamma , \\ d &= -B\cos\Phi\sin\gamma - b_1\sin\Phi\cos\gamma , \\ A &= a_1-a_2=\alpha\cos^2\theta^{+}-\delta\sin^2\theta^{+} , \\ B &= b_1-b_2=\beta_l\cos^2\theta^{-}-\beta_t\sin^2\theta^{-} . \end{aligned} \tag{3}$$

The parameters $\theta^{\pm}$ are the spin-orbit mixing parameters, given in Ref. 24. The four exchange integrals are defined as follows:

$$\begin{aligned} &\alpha=\langle R|J|R\rangle/\Omega , \quad \delta=\langle S_{\pm}|J|S_{\pm}\rangle/\Omega , \\ &\beta_t=\langle Z|J|Z\rangle/\Omega , \quad \beta_l=\langle X_{\pm}|J|X_{\pm}\rangle/\Omega , \end{aligned} \tag{4}$$

where R, $S_{\pm}$, Z, and $X_{\pm}$ represent band-edge wave functions, J is the exchange coupling constant, and γ is defined by

$$\cos^2\gamma=\frac{P_t^2}{P_l^2}\cos^2\Phi\Big/\left[\frac{P_t^2}{P_l^2}\cos^2\Phi+\sin^2\Phi\right] . \tag{5}$$

It is worth noting that for high-symmetry configurations, $\Phi=0°$ and $\Phi=90°$, the off-diagonal terms in matrix (2) vanish, and the mixing of Landau states which exists for arbitrary Φ is removed. The effect of the exchange interaction on the band states is then described simply by adding the elements a, $-a$, b, and $-b$ to the diagonal terms of the 4×4 $\mathbf{k}\cdot\mathbf{p}$ Hamiltonian.

In the low-field approximation, the only effect of the exchange interaction on the PbTe-type band structure is the modification of the g factors. The g factors then become proportional to the magnetization and to the exchange integrals a or b as follows:

$$\begin{aligned} &\bar{g}_{t,l}^{v}=g_{t,l}^{v}+\tfrac{1}{2}xS_0B_{7/2}[7\mu_{\mathrm{B}}B/k_{\mathrm{B}}(T+T_0)]a , \\ &\bar{g}_{t,l}^{c}=g_{t,l}^{c}+\tfrac{1}{2}xS_0B_{7/2}[7\mu_{\mathrm{B}}B/k_{\mathrm{B}}(T+T_0)]b . \end{aligned} \tag{6}$$

On the other hand, the low-field approximation does not predict any effect of the exchange interaction on the effective masses of the carriers. We expect, therefore, that in the Mitchell-Wallis model the exchange terms are negligible for the calculations of the cyclotron resonance energies, but should be taken into consideration in calculations of any resonance that involve the spin-flip process.

IV. EXPERIMENTAL RESULTS

A. The Faraday geometry

For the Faraday geometry (in which the magnetic field **B** and the propagation vector **q** of the incident FIR photons are both parallel to the [111] axis), two cyclotron resonances (CR's) are expected. The first of these is the CR of holes associated with the ellipsoid whose long axis is parallel to the magnetic field ($\Phi=0°$); the second one, occurring at higher fields, is the tilted orbit CR of holes from the three equivalent valleys oriented obliquely to **B** ($\Phi=70.53°$). We designate these as $\omega=\omega_c^0$ and $\omega=\omega_c^{70}$, respectively. From the cyclotron frequencies $\omega_c^{\Phi}=e\mathrm{B}/\mathrm{cm}^{\Phi}$, we can directly obtain the values of the effective masses m_{Φ} of the carriers associated with ellipsoids inclined to **B** with the angle Φ. Because the orbits associated with the tilted ellipsoids are elliptical, they can be coupled resonantly to both the CRA and the CRI circular polarization.[25] The hole orbits associated with the $\Phi=0°$ ellipsoid are circular and totally orthogonal to the exciting CRA polarization, so that the CR is only observed for the CRI excitation.

Figure 1 shows typical experimental Faraday geometry

traces of the transmission intensity for $Pb_{0.98}Eu_{0.02}Te$ as a function of magnetic field for three fixed FIR wavelengths ($\mathbf{B}\|\mathbf{q}\|[111]$), observed at $T=1.8$ K. In the CRI polarization, two resonances are clearly distinguished. The high-field resonance also appears at the same field value in the CRA polarization. As mentioned above, the resonance observed at lower fields is identified as the CR of the holes from the [111] valley parallel to **B** ($\Phi=0°$), and the minimum observed at higher fields in both CRA and CRI polarizations is the tilted orbit CR of holes located in the three valleys inclined with respect to **B** ($\Phi=70.53°$). Both resonances shift to higher fields with increasing FIR photon energy. From comparison with pure PbTe we can estimate that, for the hole concentration of 7.5×10^{16} cm^{-3}, the Fermi level is situated within the valence band, 1–2 meV below its edge.[27] At low temperatures, even in magnetic fields as low as $B=1$ T, holes occupy only the lowest Landau level 0β in each of the four valleys (β and α designating the spin states). Because of that, we can assign both observed CR's to transitions from the 0β level to the next-nearest level, 1β, with the same spin state.

Figure 2 shows a fan chart for the transition energies ($0\beta-1\beta$) versus magnetic field for the Faraday geometry. The crosses represent experimental data, and the solid lines are calculated by a fitting procedure described later in the paper.

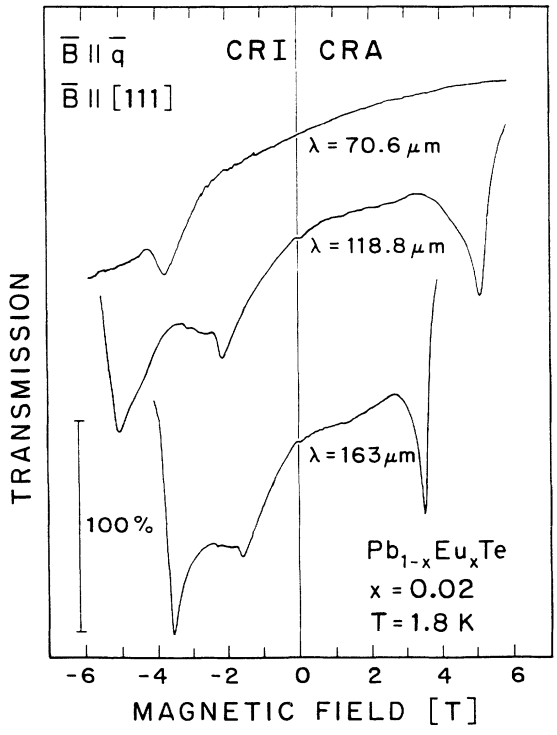

FIG. 1. FIR magnetotransmission spectra obtained on $Pb_{0.98}Eu_{0.02}Te$ in the Faraday geometry ($\mathbf{B}\|\mathbf{q}$) for CRA and CRI circular polarizations. The data were taken at $T=1.8$ K at wavelengths of 163, 118.8, and 70.6 μm. **B** was parallel to the [111] axis of the sample.

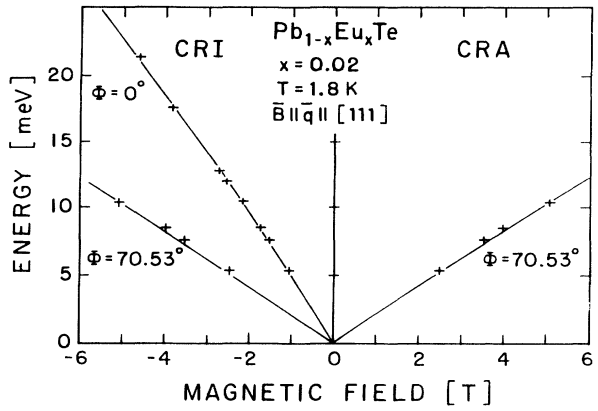

FIG. 2. Cyclotron-resonance energies vs magnetic field in $Pb_{0.98}Eu_{0.02}Te$ for CRA and CRI polarizations in the Faraday configuration. The crosses represent experimental data and the lines are calculated using the six-band model. The fitting procedure and parameters are discussed in the text. Transitions associated with the two groups of inequivalent valence-band ellipsoids, $\Phi=0°$ and $\Phi=70.53°$, are identified in the figure.

B. The Voigt geometry

In the Voigt geometry ($\mathbf{B}\perp\mathbf{q}\|[111]$), two orthogonal linearly polarized modes propagate independently: the ordinary Voigt (OV) mode, where the electric field **E** of the FIR photon is linearly polarized parallel to the external magnetic field **B**, and the extraordinary Voigt (EV) mode, where **E** is perpendicular to **B**. For the OV mode in the anisotropic multivalley system, CR arises only from those ellipsoids which are inclined with respect to **B**. The physical mechanism for the appearance of the CR in the OV mode is the tilt of the cyclotron orbit with respect to **B**. (Although cyclotron orbits are always perpendicular to **B** in momentum space, for a tilted ellipsoid the orbit is tilted with respect to **B** in real space. Thus, in executing its orbit, a carrier contributes a component of an oscillatory current parallel to **B** at the frequency ω_c^{Φ}, and can thus couple resonantly to an electric field of that frequency polarized parallel to **B**.[25])

For $Pb_{1-x}Eu_xTe$ films grown on (111) BaF_2 surfaces, there are two high-symmetry sample orientations: $\mathbf{B}\|[1\bar{1}0]$ and $\mathbf{B}\|[11\bar{2}]$. In the former case, two constant energy ellipsoids are oriented with the long axis perpendicular to **B**($\Phi=90°$). The carriers from these ellipsoids thus should not couple to the incident OV radiation. The remaining two ellipsoids are oriented obliquely to **B** ($\Phi=35.26°$). They will then give rise to a single tilted orbit CR at $\omega=\omega_c^{35}$. For $\mathbf{B}\|[11\bar{2}]$, one ellipsoid is perpendicular to **B**, one is inclined to **B** with $\Phi=61.87°$, and the remaining two are inclined with $\Phi=19.47°$. In this case, one expects to observe two resonance frequencies, ω_c^{19} and ω_c^{62}.

Figure 3 presents typical magnetotransmission spectra obtained in the ordinary Voigt configuration ($\mathbf{B}\|\mathbf{E}\perp\mathbf{q}$) for $\mathbf{B}\|[1\bar{1}0]$. The experimental picture is more complex than we predicted. At long wavelength ($\gamma=229$ μm) we observe not one but two CR's. The low-field line is the expected tilted-orbit CR of holes located in the two 35.26° valleys; the high-field line, however, arises from forbidden

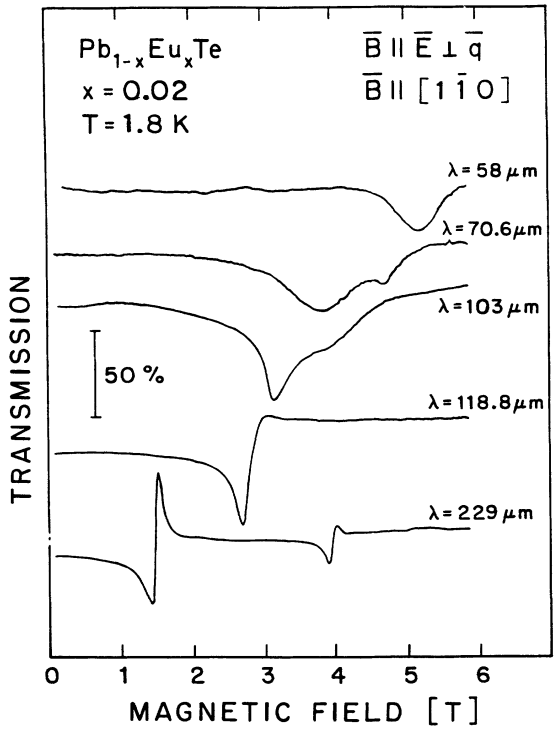

FIG. 3. FIR magnetotransmission spectra obtained on $Pb_{0.98}Eu_{0.02}Te$ in the Voigt geometry ($\mathbf{B}\perp\mathbf{q}$) for linear polarization $\mathbf{E}\|\mathbf{B}$ (OV mode). The data were taken at $T=1.8$ K for several photon wavelengths, as shown. The $[1\bar{1}0]$ axis of the sample was parallel to $\mathbf{B}$.

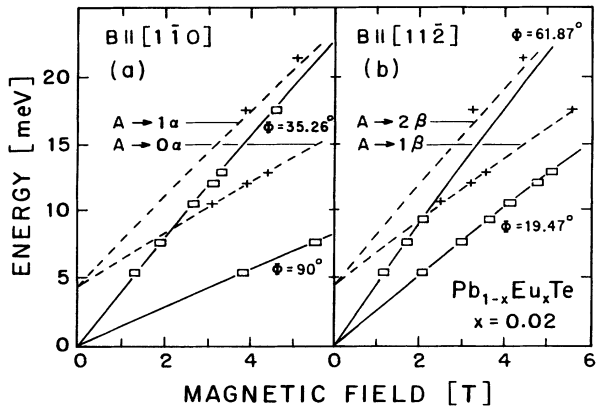

FIG. 4. Resonance transitions energies vs magnetic field in $Pb_{0.98}Eu_{0.02}Te$ for the ordinary Voigt configuration ($\mathbf{B}\|\mathbf{E}\perp\mathbf{q}$). The squares and crosses represent cyclotron resonances and transitions from the acceptor state to the valence band, respectively. The solid and dashed lines are calculated using the six-band model, with the band parameters and acceptor-state parameters discussed in the text. (a) and (b) show results for $\mathbf{B}\|[1\bar{1}0]$ and $\mathbf{B}\|[11\bar{2}]$, respectively.

transitions due to ellipsoids oriented perpendicular to $\mathbf{B}$. It is possible that this weak resonance structure arises from a small inclination of the $[1\bar{1}0]$ axis away from $\mathbf{B}$.

At shorter wavelengths in this configuration a new absorption line appears. Its linewidth δH is much larger than the observed CR linewidths, suggesting a different origin for the transition. Indeed, as will be argued later, we can interpret this structure as the transition from a shallow acceptor state to a Landau level in the valence band.

The spectra obtained for the OV configuration with $\mathbf{B}\|[11\bar{2}]$ are qualitatively similar to those shown in Fig. 3, arising simply from different inclinations of the mass ellipsoids, as discussed earlier. In Figs. 4(a) and 4(b), all the observed resonance energies in the ordinary Voigt geometry are plotted as a function of the applied field for $\mathbf{B}\|[1\bar{1}0]$ and for $\mathbf{B}\|[11\bar{2}]$, respectively. The squares represent the experimental positions of the CR's and the crosses represent the energies of the acceptor-to-band transitions. The solid and dashed lines are theoretical fits.

We now consider the second normal mode of the Voigt configuration: the extraordinary Voigt mode with $\mathbf{B}\perp\mathbf{E}$. In this geometry, in a multivalley semiconductor, up to three different kinds of CR's could be excited for each nonequivalent ellipsoid: plasma-shifted CR, incomplete screening CR, and hybrid CR.[25] In the case of our samples, however, only the incomplete screening CR has been observed. The incomplete screening effect results from nonequivalent orientation of the elliptical cyclotron orbits, which leads to incomplete screening of the internal polarization field at $\omega=\omega_c^{\Phi}$, so that orbital motion can couple to the exciting EV polarization. The other two types of CR's possible in the the EV mode (the plasma-shifted CR and the hybrid CR) are usually observed at higher frequencies, where $\omega \gg \omega_p$ [$\omega_p=(4\pi ne^2/m^*\epsilon)^{1/2}$ is the plasma frequency[25]]. For the hole concentration $n=7.5\times10^{16}$ cm^{-3}, and using parameters for pure PbTe (effective masses tensor components $m_l^v=0.3m_0$ and $m_t^v=0.02m_0$, and the optical dielectric constant $\epsilon=38$), the plasma energy corresponding to ω_p is relatively high ($\hbar\omega_p=9.4$ meV) so that the plasma-shifted and hybrid CR's are unlikely to be excited by the FIR radiation in the energy range 2.5–21 meV. It should be noted that the magnetotransmission spectra measured in the extraordinary Voigt mode have not provided any new information about the material, but only confirm the results observed in geometries already discussed. In agreement with theoretical prediction, the observed incomplete screening CR's occur at the same frequencies $\omega=\omega_c^{\Phi}$ as in the ordinary Voigt mode for the same crystal orientations.

We note parenthetically that at our longer wavelengths the transmission spectra are obtained under $\omega<\omega_p$ conditions ($\hbar\omega_p=9.4$ meV corresponds to $\lambda\cong132$ μm). This gives a valuable opportunity to investigate wave propagation under "evanescent" conditions and to observe the changes in the character of magnetotransmission as the propagation crosses over from the evanescent to the "normal" ($\omega>\omega_p$) regime. In the evanescent regime, in the Voigt configuration the CR lines display a characteristic dispersive shape (see Fig. 3, $\lambda=229$ μm). In this case the inflection point of the absorption structure corresponds to the CR field. With increasing frequency, the line shapes change to the usual absorption line form and the resonance position is determined by transmission

minima. Since our primary emphasis is on the band-structure parameters, we do not intend to analyze the above magnetoplasma phenomena in this paper.

V. ANALYSIS AND DISCUSSION

A. Cyclotron transitions: Determination of the band-structure parameters

The experimental data reported in Figs. 2 and 4 were interpreted in the framework of the six-band Mitchell-Wallis model presented in Sec. III. For the calculation of the observed $0\beta-1\beta$ CR energies, we neglected the exchange terms, for reasons discussed at the end of Sec. III. For the energy gap of $Pb_{0.98}Eu_{0.02}Te$, we assumed the value of $E_g=252$ meV already established for this composition in the literature.[10] We assumed further that the presence of the small amount of Eu in our material does not influence the far-band contributions to the effective masses and the g factors $m_t^{\pm}$, $m_l^{\pm}$, $g_t^{\pm}$, $g_l^{\pm}$ and these far-band parameters have been taken to be identical to those for pure PbTe.[26] These band parameters are very well established and yield excellent agreement with PbTe experimental data. The two remaining near-band parameters, the momentum matrix elements P_l and P_t, were determined by a least-squares fit. The best fit of the theoretical curves to the experimental points was obtained for $2P_t^2/m_o=8.23\pm0.02$ eV and $2P_l^2/m_0=0.55\pm0.02$ eV. The result for the fitting procedure is shown in Figs. 2 and 4. The excellent agreement of the theoretical curves with the data shows that the six-band model (without the exchange terms) is well suited for the calculations of the CR energies in $Pb_{1-x}Eu_xTe$.

As compared to PbTe, where the anisotropy of the near-band parameters P_t^2/P_l^2 equals 10.3, the presence of even a small amount of Eu in the $Pb_{0.98}Eu_{0.02}Te$ lattice increases the anisotropy significantly, resulting in the value of 14.9. It is interesting that it is the transverse matrix element which is strongly affected by the presence of Eu (and scales approximately with the energy gap), but the longitudinal matrix element appears unaffected [for PbTe the matrix element values are $2P_t^2/m_0=5.9$ eV, $2P_l^2/m_0=0.57$ eV (Ref. 26)]. The increase of the band anisotropy has also been reported for $Pb_{1-x}Mn_xTe$ with increasing content of Mn. In that case, however, both P_l and P_t were affected by the presence of Mn.[22,23] On the other hand, no significant influence of Eu on the momentum matrix elements have been observed in $Pb_{1-x}Eu_xSe$.[12]

B. Acceptor-to-valence-band transitions and determination of exchange constants

Taking into account the band parameters obtained from CR energies, we are able to interpret the additional broader absorption lines observed in the Voigt geometry, whose energies are shown by the crosses in Figs. 4(a) and 4(b). These energies do not extrapolate to zero for $B=0$ T, indicating that the transitions initiate not from a band state but from a state located within the gap, probably from a shallow acceptor. The identification of the final states of those transitions is based on the observation that the magnetic-field splittings of the observed lines are almost identical for both crystal orientations [compare Figs. 4(a) and 4(b)]. This experimental fact suggests that the final states of the observed transitions belong to those band ellipsoids which are inclined with respect to **B** by the same angle for both orientations, i.e., ellipsoids which are perpendicular to **B** ($\Phi=90°$). Additional corroboration of this interpretation is provided by comparing the relative intensities of the absorption lines for $\mathbf{B}\|[1\bar{1}0]$ and $\mathbf{B}\|[11\bar{2}]$ configurations. In the former case, two ellipsoids are oriented perpendicular to **B** and the absorption intensity of the line under discussion is approximately twice as strong as in the latter configuration, where there is only one ellipsoid of such orientation. Taking into account these considerations, we calculate the transition energies from a single shallow acceptor state to the lowest unoccupied Landau states, as marked in Figs. 4(a) and 4(b). The band parameters are taken from the theoretical fits to the CR energies presented above. The activation energy of the acceptor was assumed to be a linear function of the magnetic field. The best fit was obtained for $E_A=4.4+0.9B$ meV (where B is given in T), relative to the bottom of the valence band at zero field. The theoretical curves resulting from this analysis (dashed lines in Figs. 4) are in rather good agreement with the experimental points. Note that the activation energy in zero magnetic field obtained from the fit, $E_A=4.4$ meV, is very close to the value obtained from transport measurements, i.e., $E_A=4.2$ meV.

It is important to note that the acceptor-to-band transitions are very sensitive to the crystal orientation: for $\mathbf{B}\|[1\bar{1}0]$ the final states are spin "up" (designated as α states), whereas the $\mathbf{B}\|[11\bar{2}]$, final states are spin "down" (β states). The selection rules reflect the strong anisotropy of the system.

Comparison of the energies of A-1α and A-1β transitions directly provides the value of the g factor for the first Landau $\Phi=90°$ valleys and, consequently, information about the exchange interaction between the Eu^{2+} ions and the holes. The g factor deduced from this comparison, $\bar{g}_t^v=15.9\pm1.0$, is very close to the value calculated from the band parameters established on the basis of the CR measurements, $g_t^v=17.3\pm1.0$ [Eq. (1)], although the discrepancy between them only slightly exceeds the experimental error, $\Delta g=\bar{g}_t^v-g_t^v=-1.4\pm1.0$. In order to establish an upper limit for the exchange integral α, we have assumed that the difference between g_t^v and $\bar{g}_t^v$ is caused by the exchange interaction which, according to Eq. (6) for $\Phi=90°$, is given by $\Delta g=\frac{1}{2}xS_0B_{7/2}(\ )\alpha\cos^2\theta^+$. Using the known magnetization data[14-16] and taking $\cos^2\theta^+=0.957$,[25] we deduced the value of α corresponding to this Δg as $\alpha=-7.5\pm5.5$ meV. As already stated, because of the experimental uncertainty of Δg, the result should be regarded as the upper limit for α rather than its actual value. This result indicates that α for $Pb_{1-x}Eu_xTe$ is much smaller than for $Pb_{1-x}Mn_xTe$ [$\alpha\cong-300\pm15$ meV (Ref. 23)] and for $Pb_{1-x}Eu_xSe$ [$\alpha\cong60$ meV (Ref. 12)].

Magnetotransmission measurements at higher temperatures provide additional corroboration that α is very

small. The resonance positions of all observed resonances are completely independent of temperature, in contrast with magneto-optical data in other DMS's. Given the sharpness of the resonances (resonance positions can be determined to at least 1% of the resonance field even at $T=60$ K) we can conclude that the exchange interaction in $Pb_{0.98}Eu_{0.02}Te$ is so weak that its contribution to the energies of the magneto-optical transitions is within the experimental error of the present experiment, consistent with the small value obtained in the preceding paragraph.

The integral α determines the influence of the exchange coupling on the s-type wave function, which is the dominant part of the entire function of the valence-band edge. The d-type contribution to the valence-band-edge wave function and, consequently, the component $a_2=\delta\sin^2\theta^+$ of the exchange integral, are expected to be very small in $Pb_{0.98}Eu_{0.02}Te$ because the spin-orbit mixing parameter θ^+ is small in PbTe [$\sin^2\theta^+=0.043$ (Ref. 24)]. Furthermore, we can expect that, as in the case of other IV-VI–based DMS's, the exchange integrals of the valence band are significantly bigger than those of the conduction band.[12] If α indeed describes the dominant part of the exchange interaction in $Pb_{0.98}Eu_{0.02}Te$, the effect of this interaction on the band states is practically negligible. The energy diagram of $Pb_{0.98}Eu_{0.02}Te$ for $\mathbf{B}\|[1\bar{1}0]$ presented in Fig. 5 could be the best illustration for this conclusion. The lines in Figs. 5(a) and 5(b) represent the calculated energies of several lowest Landau levels in the valence band as a function of magnetic field for ellipsoids oriented perpendicular ($\Phi=90°$) and tilted by the angle $\Phi=35.26°$ with respect to $\mathbf{B}$, respectively. The magnetic-field dependence of the energy of the acceptor state is also shown. In the calculations we have used the band and acceptor parameters reported above. The vertical arrows correspond to the four types of transitions presented in Fig. 4(a). The energies of the Landau levels calculated with the exchange terms included differ from those calculated without the exchange terms by less than 0.4 meV in the entire range of magnetic fields, which corresponds roughly to the thickness of the lines representing the positions of the Landau levels in the figure.

The small values of exchange integrals are in good agreement with both experimental and theoretical predictions. Based on magnetization measurements [the nearest-neighbor exchange constants in $Pb_{1-x}Eu_xTe$ are smaller than those in $Pb_{1-x}Mn_xTe$ (Refs. 14–16)], one expects that the exchange interaction between free holes and Eu ions is much smaller than the interaction between free holes and Mn ions in $Pb_{1-x}Mn_xTe$ alloys. The theoretical calculations of the exchange interaction in $II_{1-x}Mn_xVI$ DMS's point out the importance of the hybridization of the $3d^5$ magnetic levels with the p-band electrons.[28] For $Pb_{1-x}Eu_xTe$ the valence-band electrons are described predominantly by p orbitals while the magnetic level is $4f^7$. In that case the hybridization is expected to be very weak, thus resulting in small values of the exchange integrals.

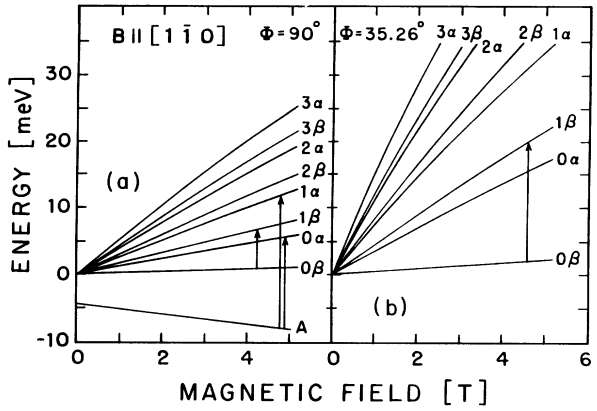

FIG. 5. Magnetic-field dependence of the shallow acceptor-state A and low-index Landau states in the valence band of $Pb_{0.98}Eu_{0.02}Te$. The curves are calculated with the parameters obtained from the preceding fits. The left half (a) is for $\Phi=90°$, the right half (b) is for $\Phi=35.26°$. The arrows represent the four types of resonance transitions observed in the Voigt geometry for $\mathbf{B}\|[1\bar{1}0]$, corresponding to the data plotted in Fig. 4(a).

VI. CONCLUSIONS

FIR magnetotransmission measurements have been performed on MBE-grown $Pb_{1-x}Eu_xTe$ films with $x=0.020$. It was established that the six-band $\mathbf{k}\cdot\mathbf{p}$ Mitchell-Wallis model provides an excellent base for the theoretical description of the magneto-optical data. The near-band parameters of this model were experimentally determined to be $2P_t^2/m_0=8.23\pm0.02$ eV and $2P_l^2/m_0=0.55\pm0.02$ eV, indicating a strong increase of the band anisotropy even for this small Eu content, as compared to pure PbTe. As expected from magnetization experiments, the free-hole–Eu-exchange interaction in $Pb_{1-x}Eu_xTe$ is at least one order of magnitude weaker than the free-hole–Mn interaction in $Pb_{1-x}Mn_xTe$. The dominant component of the valence-band exchange integral α which determines the influence of the exchange coupling on hole states described by s-type wave functions was established to be small, with absolute value smaller than 7.5 ± 5.5 meV. We have thus established that the exchange interaction in $Pb_{0.98}Eu_{0.02}Te$ is very weak, so that in the presence of magnetic field the band structure of this material can be accurately described by the Mitchell-Wallis model without the exchange terms.

ACKNOWLEDGMENT

The work was supported by National Science Foundation Grant No. DMR-8904802.

*On leave from the Institute of Physics, Polish Academy of Sciences, Warsaw, Poland.

[1]D. L. Partin, Appl. Phys. Lett. **43**, 996 (1983).

[2]W. Goltsos, J. Nakahara, A. V. Nurmikko, and D. L. Partin, Appl. Phys. Lett. **46**, 1173 (1985).

[3]Z. Feit, D. Kostyk, R. J. Woods, and P. Mak, Appl. Phys. Lett. **58**, 343 (1991).

[4]K. H. Schlereth, H. Böttner, and M. Tacke, Appl. Phys. Lett. **56**, 2169 (1990).

[5]J. K. Furdyna, J. Appl. Phys. **64**, R29 (1988), and references cited therein.

[6]*Diluted Magnetic Semiconductors, Semiconductors and Semimetals,* edited by J. K. Furdyna and J. Kossut (Academic, Boston, 1988), Vol. 25.

[7]C. Paparoditis and R. Suryanarayanan, J. Cryst. Growth **13/14**, 389 (1972).

[8]D. L. Partin, IEEE J. Quantum Electron. **QE-24**, 1716 (1988).

[9]A. Ishida, S. Matsuura, M. Mizuno, Y. Sase, and H. Fujiyasu, J. Appl. Phys. **63**, 4572 (1988).

[10]R. Suryanarayanan and S. K. Das, J. Appl. Phys. **67**, 1612 (1990).

[11]R. Suryanarayanan and C. Paparoditis, J. Phys. (Paris) Colloq. **29**, C4-46 (1968).

[12]P. Röthlein, H. Pascher, G. Bauer, and M. Tacke, Semicond. Sci. Technol. **5**, S147 (1990).

[13]J. W. Tomm, K. H. Herrmann, H. Bötner, M. Tacke, and A. Lambrecht, Phys. Status Solidi A **119**, (1990).

[14]G. Braunstein, G. Dresselhaus, J. Heremans, and D. L. Partin, Phys. Rev. B **35**, 1969 (1987).

[15]M. Górska, J. R. Anderson, G. Kido, and Z. Golacki, Solid State Commun. **75**, 363 (1990).

[16]M. Górska and J. R. Anderson, Phys. Rev. B **38**, 9120 (1988).

[17]D. L. Mitchell and R. F. Wallis, Phys. Rev. **151**, 581 (1965).

[18]J. O. Dimmock, in *The Physics of Semimetals and Narrow Band Semiconductors,* edited by D. L. Carter and R. T. Bate (Pergamon, Oxford, 1971), p. 405.

[19]M. S. Adler, C. R. Hewes, and S. D. Senturia, Phys. Rev. B **7**, 186 (1973).

[20]G. Bauer, in *Narrow Gap Semiconductors: Physics and Applications,* edited by W. Zawadzki, Springer Lecture Notes in Physics Vol. 133 (Springer, Berlin, 1980), p. 427.

[21]J. Niewodniczańska-Zawadzka, J. G. Elsinger, L. Palmetshofer, A. Lopez-Otero, E. J. Fantner, G. Bauer, and W. Zawadski, Physica B+C, **117&118B**, 458 (1983).

[22]H. Pascher, P. Röthlein, G. Bauer, and M. von Ortenberg, Phys. Rev. B **40**, 10469 (1989).

[23]H. Pascher, P. Röthlein, G. Bauer, and L. Palmetshofer, Phys. Rev. B. **36**, 9395 (1987).

[24]R. L. Bernick and L. Kleinman, Solid State Commun. **8**, 569 (1970).

[25]E. D. Palik, J. K. Furdyna, Rep. Prog. Phys. **33**, 1193 (1970).

[26]G. Appold, R. Gisar, G. Bauer, H. Burkhard, R. Ebert, H. Pascher, and H. G. Hafele, in *Proceedings of the International Conference on the Physics of Semiconductors, Edinburgh,* edited by B. L. H. Wilson (The Institute of Physics and the Physical Society, London, 1978), p. 1101.

[27]M. Grudzień and A. Rogalski, Acta Phys. Pol. A **58**, 765 (1980).

[28]A. K. Bhattacharjee, G. Fishman, and B. Coqblin, Physica **117&118** 449 (1983).